Controls of lithology and degree of fracturing on the in-situ estimation of rock mass hardness using the Equotip hardness tester

Elisa Mammoliti[a], Sara Ciattoni[b], Mirko Francioni[b]*, Gregorio Baiocchi[c], Veronica Gironelli[c], Stefano Mazzoli[c]

[a]*Dipartimento di Scienze, Ingegneria della Materia dell'Ambiente ed Urbanistica (SIMAU), Università Politecnica delle Marche, Via Brecce Bianche 12, 60100 Ancona, Italy;*
[b]*Dipartimento di Scienze Pure e Applicate (DiSPeA), Università di Urbino "Carlo Bo", Via Aurelio Saffi, 2, 61029 Urbino, Italy.*
[c]*Scuola di Scienze e Tecnologie, Sezione di Geologia, Università di Camerino, via Gentile III da Varano, 62032 Camerino, Italy.*
**corresponding author: mirko.francioni@uniurb.it (M.F)*

Abstract

The use of the Equotip hardness tester in engineering geology has increased significantly in recent years, especially in estimating the strength of weak and weathered rock materials. Weathering and fracturing, besides lithology, influence the overall behaviour of the rock mass and the response of the non-destructive tester. In this study, more than 9,000 Equotip rebound measurements were collected from twelve rock outcrops of several geological formations in central Italy, using a regular measurement grid approach. In addition, linear scan lines were combined with the analysis of photogrammetric sampling windows to determine geomechanical indexes such as Rock Quality Designation (RQD), Joint Volumetric Count (Jv) and Fracture intensity (P21) to be coupled with the Equotip measurements. A strong correlation was found between RQD, Jv, P21 and the Equotip rebound. The study presents an innovative approach by integrating extensive Equotip rebound measurements with geomechanical indices (RQD, Jv, P21) and advanced photogrammetric techniques. This combination provides new quantitative constraints on the relationship between fracture intensity, lithological variation, and mechanical properties of rock masses. Our findings highlight the potential of Equotip testing as a fast and reliable tool for in-situ rock mass quality assessment, also in heterogeneous geological settings, improving hazard management and engineering design.

Keywords: Equotip; RQD, Jv, P21, rock mass fracturing; discontinuities; mechanical layering

1. Introduction

Rock strength refers to the innate strength of an isotropic rock in particular conditions, both in wet and dry conditions. It can be measured in the laboratory through uniaxial or triaxial tests, as well as in the field with non-destructive rebound devices. Accurate measurement of rock mass strength is critical for a wide range of geotechnical applications, including slope stability, tunnelling, and foundation design. Traditional methods, such as uniaxial compressive strength tests and triaxial tests, are well-established but often require extensive sample preparation and can be destructive, making them less suitable for large-scale field assessments. Furthermore, the presence of

discontinuities, weathering, and structural complexities in rock masses can significantly influence their mechanical behavior, creating challenges in scaling laboratory results to in-situ conditions. Consequently, non-destructive methods have gained increasing importance in recent years, providing more practical solutions for large-scale and in-situ applications. Moreover, the principle of isotropy generally applied to rock samples is not applicable to rock masses due to the scale effect (Palmstrom 2005) and the presence of discontinuities that affect overall rock behaviour and stability (Einstein et al. 1983; Shang et al. 2018; Kim & Leon 2019; Mammoliti et al. 2022). Bulk properties cannot be easily generalised and usually require a large number of destructive tests to obtain a representative value of a significant rock exposure (Arman et al. 2013).

In this context, non-destructive testing methods, such as rebound devices, have emerged as valuable tools for estimating *in-situ* rock mass properties. To the best of the authors' knowledge, the Schmidt hammer is the most widely used tool for estimating rock mass properties, and extensive literature is available on its applications (Greco and Sorriso-Valvo 2005; Katz et al. 2000; McGinnis et al. 2017; Morris et al. 2009; Shackleton et al. 2005; Torabi et al. 2018 and literature therein). However, one of the limitations of the Schmidt Hammer is its relatively high impact energy (0.735 N/m for the L-type hammer and 2-207 N7m for the N-type hammer) (Viles et al. 2011), which make it unsuitable for weak and very friable materials which can be damaged by the rebound. In fact, as reported by Aoki and Matsukura (2007a), although the Schmidt hammer could be used to rocks with a minimum strength of 20 MPa, this is usually used to cover the range of medium to hard rocks (50-150 MPa). In contrast, the Equotip hardness tester (EQ), which was originally developed by Proceq s.r.l. in the 1970s for non-destructive testing of metals, with its lower impact energy (11 N/mm) is capable of measuring a broader spectrum of rock types, from extremely weak materials to very strong ones. Recent advancements have positioned the EQ as a promising substitute for the traditional Schmidt hammer, demonstrating its effectiveness across a broad spectrum of materials. It is mainly used for determining the uniaxial compressive strength of the intact rock (Uniaxial Compressive Strength, UCS) and discontinuities (Joint Compressive Strength, JCS, Barton 1973; Barton and Choubey 1977; Yilmaz 2013; Yilmaz & Goktan 2019) based on the rebound principle that provide reliable and highly effective measurements. This includes applications for very low-strength materials with UCS below 0.1 MPa (Mammoliti et al., 2021) and extends to extremely hard materials with

UCS exceeding 200 MPa (Aoki and Matsukura, 2008; Coombes et al., 2013 Guan et al., 2024). The low impact energy of the EQ also permits to detect minor changes in rock hardness (Aoki and Matsukura 2007b; Viles et al. 2011; Alberti et al. 2013; Ritz et al. 2014; Thrower et al. 2022). EQ has been widely employed in rock mechanics studies for assessing the mechanical properties of rock specimens under controlled laboratory conditions (Furuya et al., 2015; Liu et al., 2020; Aldeeky et al., 2020; Sakız, 2024; Tasse et al., 2024). However, its use for in-situ assessments has been mostly limited to geomorphological studies (Alberti et al., 2013; Viles et al., 2013; Pappalardo et al., 2018; Wasaka et al., 2006) and to evaluate the decrease in rock hardness due to weathering (Viles et al., 2011; Ritz et al., 2014; Wilhelm et al., 2016; Desarnaud et al., 2019; Mammoliti et al., 2024), as well as to assess the excavatability of rocks in tunneling (Tsusaka & Tokiwa, 2013). To the best of the authors knowledge, its potential for characterizing the mechanical properties of layered and faulted and/or jointed rocks has not yet been widely exploited. With this premise, the purpose of this study is to evaluate the suitability of the *in-situ* EQ hardness tester for rock mass zoning evaluations based on degree of fracturing and lithology variation. Correlation between EQ rebound and several geomechanical indices representing the fracturing degree of rock masses, including Jv, RQD and P21 have been assessed analysing twelve different outcrops within the Umbria-Marche stratigraphic sequence. Fracture parameters for each outcrop were determined by coupling 1D scan lines with low-cost photogrammetric analysis (Francioni et al. 2019) and correlated with average EQ values obtained from field data collection using a regular measurement grid on the outcrops. The potential uses of EQ to define rock mass strength were evaluated and discussed as well as the role of fracture intensity and lithology.

2. Geological framework of the tested areas

A selection of outcrops from the Umbria-Marche succession were chosen in central and northern Apennines, as illustrated in Fig.1. These include the Fiastra area in the Marche Region (Fig. 1b) and the Montagna Dei Fiori area (MDF) in the Abruzzi Region (Fig. 1c). From a morphotectonic point of view, the regions lie in the southern part of the Umbria-Marche Apennines and the foothills. The Apennines were formed by the convergence of Corsica-Sardinia's continental margins (which are of Eurasian plate pertinence) to the west with Adria (which has African

affinity) to the east. The deepest geological units, namely the Paleozoic crystalline basement and the overlying phyllites and Permo-Triassic continental siliciclastic units, commonly referred to as the Verrucano Group, are not outcropping in the Apennines. The overlying pre-orogenic sedimentary succession is characterised at its base by Upper Triassic evaporites (Burano Anhydrides Fm.). The uppermost Triassic to Eocene portion of the Umbria-Marche Stratigraphic Succession is dominated by carbonates and approximately 2000 metres thick. The bottom layer consists of the Calcare Massiccio Fm., and the top layer is the Scaglia Rossa Fm. (as shown in Fig. 1). The Scaglia Rossa Formation is located beneath a 2000/2500 m thick layer of predominantly marly and terrigenous marine deposits dating from the Late Eocene to the Plio-Pleistocene, followed by late Quaternary continental deposits.

In the Northern and Central Apennines, the thrust belt is characterised by an arcuate shape and the prevalence of asymmetrical anticlines, which are mostly faulted and predominantly verging towards the northeast, involving a succession of Mesozoic-Tertiary sedimentary units (Calamita and Deiana 1986). The Olevano-Antrodoco-Sibillini Mts. and Gran Sasso thrusts (Fig. 1a) represent the Umbria-Marche and Latium-Abruzzi Apennine main mountain fronts (Calamita et al. 2021). In their footwall, contractional structures such as the Acquasanta and Montagna dei Fiori (MDF) anticlines involve the pre-orogenic Mesozoic carbonate succession in the fold core. The MDF anticline is an overturned fold produced by early Pliocene folding and thrusting involving the Jurassic-Miocene Umbria-Marche carbonate succession and the unconformably overlying siliciclastic foreland basin deposits of the Messinian Laga formation (Fm.) (e.g., Calamita et al. 1998; Di Francesco et al. 2010; Mattei 1987; Scisciani et al. 2002; Mazzoli et al. 2002; Scisciani and Montefalcone 2006; Tozer et al. 2006; Storti et al. 2017). The crestal zone of the MDF anticline is affected by a ca. 10 km long, SW-dipping fault juxtaposing the Miocene Marne con Cerrogna Formation (CRR, Fig. 1c) and the pre-orogenic carbonate succession (Mattei 1987; Mazzoli et al. 2002; Scisciani et al. 2002). The territory of MDF (Fig. 1c) has extraordinary rocky outcrops that represent the Umbria-Marche stratigraphy along the MDF anticline, in which four geomechanical measurement sites (Table 1) are located in the Corniola Fm (ID 1, COI, Lower Jurassic), Calcari Diasprigni and Salinello Fms. (ID 2, CDU, Upper/Mid Jurassic), Marne a Fucoidi Fm. (ID 3, FUC; Lower Jurassic), and Scaglia Rossa Fm. (ID 4, SAA, Upper Cretaceous-Oligocene). In the Fiastra area (Fig. 1b), which is located within the main carbonate ridge to the west (in the hanging wall of the Olevano-Antrodoco-

Sibillini Mts. Thrust), a total of eight geomechanical measurement sites (Table 1) are located in the Scaglia Bianca Fm. (ID 11, SBI, Upper Cretaceous) and Scaglia Rossa Fm. (ID from 5 to 12, SAA, Upper Cretaceous-Eocene). The geological formation (Fms.) analysed in this work are all composed of a single lithology, with the exception of ID 111 (SBI), which is characterised by marly limestones with thin alternations of marls, and ID 3 (FUC), consisting of marls, shaley marls and marly limestones with abundant clay levels.

Table 1 Description of the geological formations tested (modified from Pierantoni et al., 2013)

Geomechanical measurement site (ID)	**Geological formation**	**Age**	**Description**
4, 5, 6, 7, 8, 9, 10, 12	Scaglia Rossa Fm. (SAA)	Lower Turonian p.p. – Lutanian p.p.	Pink, red, dark, rarely white marly limestones, stratified in medium beds, with very thin pelitic levels and red or pink chert in nodules and ribbon missing in the middle part. The latter contains thick marly levels.
11	Scaglia Bianca Fm. (SBI)	Upper Albian p.p. – Lower Turonian p.p.	Whitish limestones and marly limestones, in middle beds, with chert beds and ribbons, black or brown in the upper part, pink in the lower one. In the lower part, thin beds of marls are present.
3	Marne a Fucoidi Fm (FUC)	Lower Aptian p.p. – Upper Albian p.p.	Grey, green and red marls and shaly marls, marly limestones with abundant clay levels, frequently bituminous (black shales).
2	Calcari Diasprigni Fm. and Formazione del Salinello (CDU)	Upper Bajocian – Lower Tithonian	Calcarenites, 30–50 cm thick beds with gray cherts and siliceous calcilutites with green cherts.
1	Corniola Fm. (COI)	Lower	Micrite limestone and 10–80 cm thick calcarenites

		Sinemurian p.p. – Lower Toarcian p.p.	beds with localised dolomites.

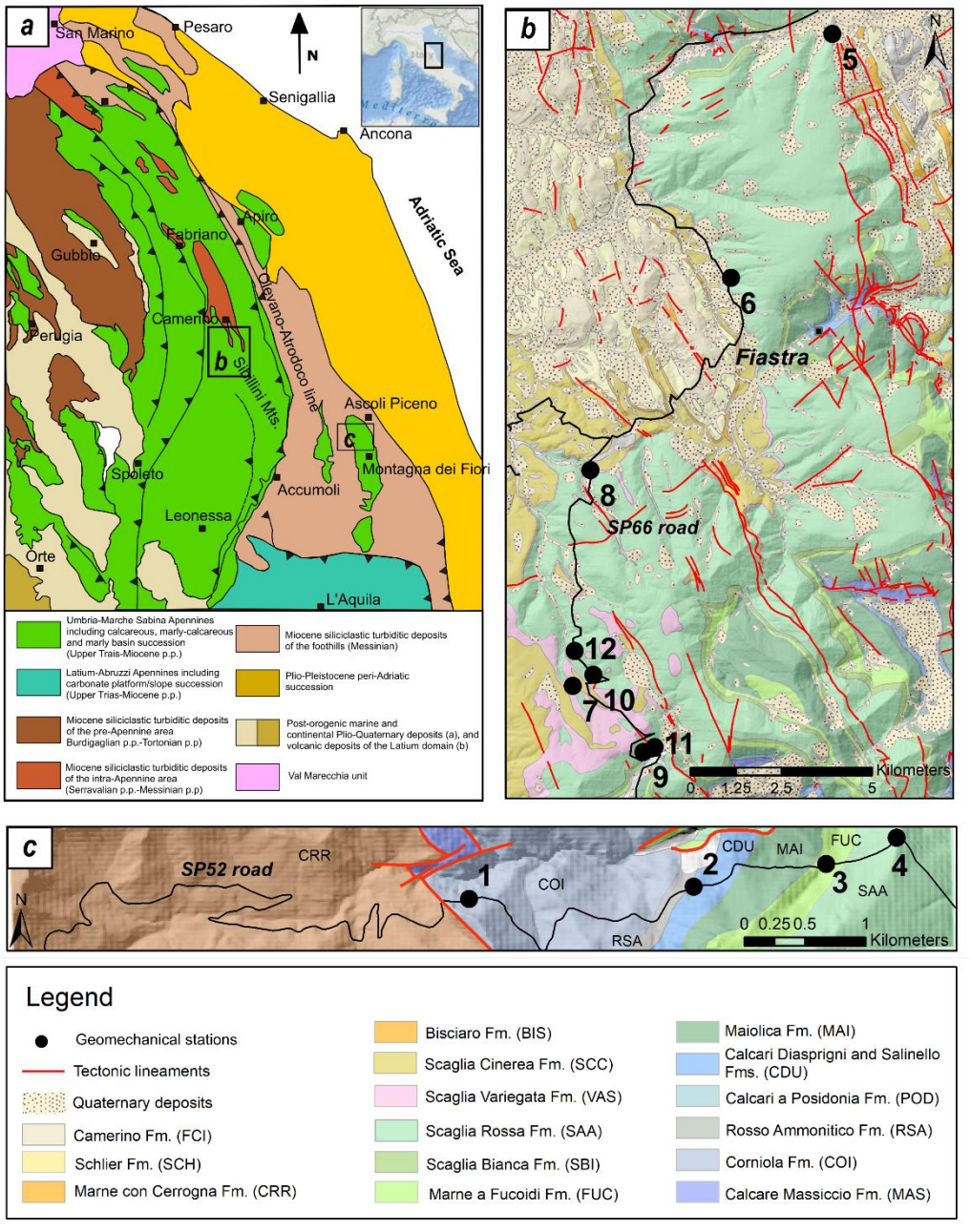

Fig 1 a Geological sketch map of the Umbria-Marche Apennines (modified after Pierantoni et al., 2013); **b** Fiastra area; **c** Montagna Dei Fiori area (modified from Francioni et al. 2019). The location and identification code (ID) of the investigated outcrops are reported

3. Methodology

The methodology presented in this research combines traditional geomechanical indices (RQD, Jv, P21) with an extensive grid-based collection of EQ rebound data. The geomechanical analysis was supplemented by photogrammetric surveys to enhance fracture network characterization at the site scale.

3.1. Geomechanical analysis of the fracture network

The geomechanical analysis of the fracture network was carried out on 12 different outcrops (Table 1) along the SP52 road in the Fiastra area (outcrops ID 5-12) and the SP66 road in the MDF area (outcrops ID 1-4) (see Fig. 1b, c). The MDF anticline axial plane is intersected orthogonally by the SP52 road, which displays multiple geological formations belonging to the Umbria-Marche stratigraphic succession (see Fig. 1 and Table 1). The selected rock outcrops in both areas exhibit several lithological characteristics, which are detailed in Table 1. These outcrops are composed of multilayered rock masses with varying geomechanical characteristics. For the assessment of the degree of fracturing, the primary method entailed measuring fractures along linear traverses (scan lines), oriented orthogonally to at least one set of discontinuities. The scan line length was determined based upon outcrop length, varying between 2 m and approximately 15 m. To prevent orientation bias of the discontinuities during the survey, various scan line orientations were used. Outcrops with a restricted range of bed thickness were chosen to mitigate the influence of mechanical layer thickness (Guerriero et al. 2015), which governs fracture density. This data set is used to compute geomechanical indices representing the density of discontinuities along the scan lines, such as the RQD (Deere 1963) and the Jv, expressed as:

$$RQD = \frac{\sum L > 10cm}{total\ length\ of\ scanline} \times 100$$

where L is the apparent length among consecutive discontinuities in the scan line

$$Jv = \sum \frac{1}{S1} + \frac{1}{S2} + \frac{1}{S3}$$

where, for three discontinuity sets, S_n is the spacing of each set.

3.2. Photogrammetric survey

The P21 is defined as the fracture trace length per unit area (m/m^2) and is one of the most used parameters for rock mass characterization that can be easily derived from photogrammetric survey (Mammoliti et al. 2023). In this work, the P21 has been determined through orthophotos resulting from the photogrammetric approach proposed by Francioni et al. (2019), using a handheld camera. This method involves capturing a sequence of photographs with a minimum overlap of about 80% by applying the image fan technique, which continuously changes the line of sight (Birch, 2006) and georeferencing using a known geometric square (Francioni et al. 2019). The 3D model was created with Metashape software and georeferenced using local coordinates, assuming one vertex of the square is 0, 0, 0. To determine the fracture intensity parameter (P21 - expressed as fracture length per m^2), NetworkGT toolbox for ArcGIS (Nyberg et al. 2018) was used to identify discontinuities (Fig. 2), following the method introduced by Dershowitz and

196 Herda (1992).

197

198 **Fig. 2** Example of P21 calculation using the NetworkgGT tool of ArcGIS
199

200 *3.3. Data collection with the EQ*

201 A compact version of the EQ, called Piccolo 2 (Proceq 1977), was chosen to test the rock quality in several outcrops
202 with different fracture density values. The EQ is a rebound based instrument that has some advantages over the classic
203 Schmidt hammer. Indeed, due to its lower impact energy (IE = 11 N/mm, i.e., about 1/66 of the L-type SH), it can be
204 used on a wider range of rock materials, from extremely weathered and weak materials with UCS < 0.1 MPa
205 (Mammoliti et al., 2021) to unweathered fresh rocks (Aoki and Matsukura 2008; Coombes et al. 2013; Hujer et al.
206 2014). Proceq (1977) recommend that the impact should be perpendicular to the rock face when measured, and the
207 rock surface must be adequately cleaned and smoothed with carborundum before testing. To avoid the negative effects
208 of moisture content on rebound (Sumner and Nel 2002), all data collection was carried out in dry conditions. EQ data
209 were collected on the outcrop using a measurement grid with equally spaced intervals, covering the same extent of

the scan lines. The grid is made up of equally spaced (approximately 20 x 20 cm) nodes (Fig. 3), for which a total of 40 measurements are taken for each node using the repeated impact method. If the outcrop consists of more than one lithology, the measuring nodes shall be distributed over the outcrop in proportion to the percentage of each lithology and a weighted average of rebound value was calculated for each node.

The method has been developed to collect a significant number of measurements over the entire rock mass. This approach yields a representative statistic of the rock mass's overall quality and overcomes the problem of the scale effect. Lavg is a numerical, dimensionless measure of rock mass hardness, and can be converted to rock strength if a correlation equation with the UCS is available.

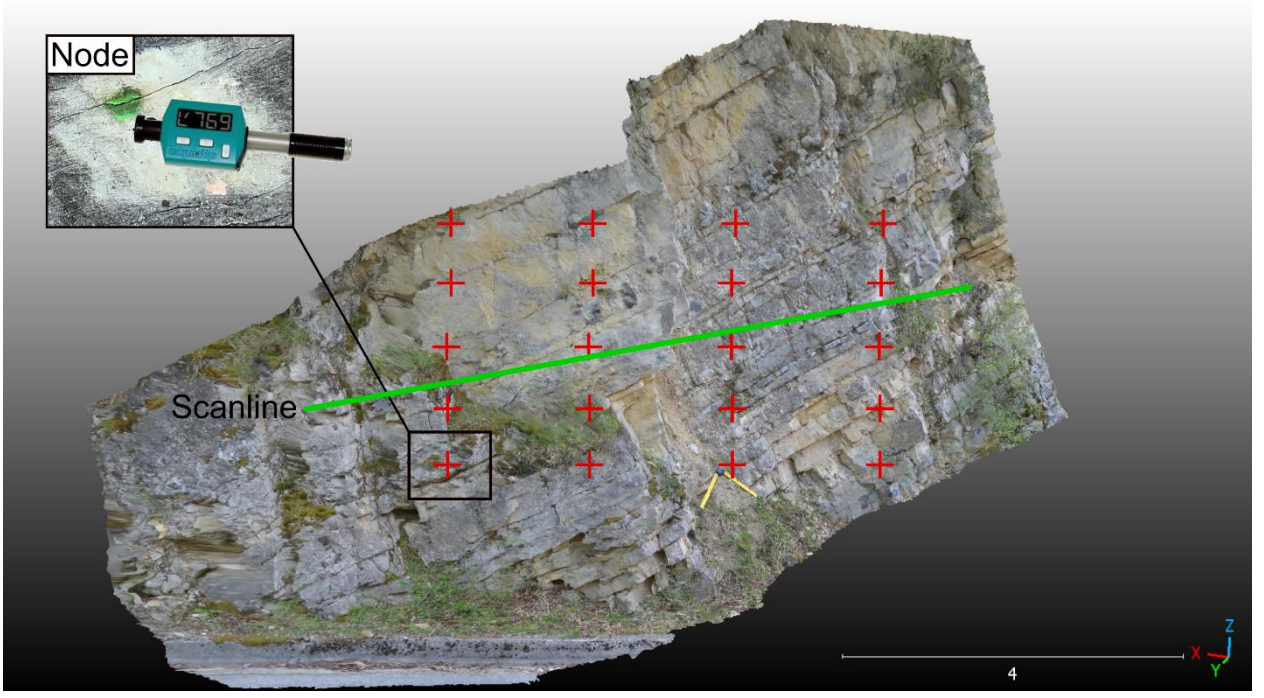

Fig. 3 Example of measuring grid used to collect data with the EQ on a rock outcrop composed by one single lithology. Red crosses represent the nodes of the grid, while the green line represents the 1D scan line

4. Results

4.1. Fracture network results

During the geomechanical analysis, over 1,300 measurements of discontinuity orientation were collected in Fiastra and MDF areas (Fig. 4 and Table 2). In the Fiastra area, two main joint sets oriented NW-SE and NE-SW (J1 and J2 in Fig. 4a), almost vertical and predominantly orthogonal to the bedding plane (S0, Fig 4a) are identified in the SBI and SAA Fms. The NE-SW joint set (J1 in Fig. 4a) includes joints with variable openings as well as extensional veins filled with calcite, while the NW-SE joint set (J2 in Fig. 4a) includes the dissolution cleavage, characterized by a tight, sawtooth-like morphology reminiscent of tectonic stylolites. From a geostructural perspective, the relationship of J1 and J2 to the bedding suggests that cleavage from dissolution and joints perpendicular to it were formed in layers that were still horizontal, i.e. thus prior to the amplification of the folds affecting the Umbria-Marche stratigraphic

succession in the study area. The discontinuity sets in the Fiastra present a constant orientation and therefore have been included in a single stereonet. In the MDF area, two joint sets J1 and J2, striking orthogonal to the bedding, are identified in the COI, CDU, FUC and SAA Fms (Fig. 4b) and interpreted as extensional joint sets (Watkins et al., 2018). The stereonets in this case have been created for each formation due to the influence of the MDF anticline. In Table 3, the main joint sets and the geomechanical indices are reported for each geological formation, coupling data of both the study areas. The data presented in Table 3 shows a high variability of RQD, Jv and P21 in the dataset; in details, the RQD ranges between 31% and 81%, the Jv between 12 and 26 and the P21 between 9 and 19. The variability of fracturing data strongly reflects the lithology and structural characteristics. In fact, geological formations characterised by limestones bed alternating with marls (SR, FUC, SBI) presents higher fracturing degree (Jv ranging from 11.5 to 26, RQD from 31 to 72 and P21 from 12.7 to 19) while the geological formation mainly composed by one lithology (COI, CDU) lower Jv (6.7 and 10.6), RQD (81 and 80) and P21 (9 and 9.1) are observed.

Table 2 Dip and dip direction of the discontinuity sets measured in Fiastra and MDF areas, with number of observations and Fisher K-value

ID	Geol. Fm	Discontinuity set	Dip/Dip direction (°/°)	No. of observations	Fisher K-value
1	COI	J1	77/339	47	28
		J2	69/256	59	22
		S0	31/77	58	51
2	CDU	J1	54/264	59	15
		J2	74/336	48	28
		S0	36/66	45	28
3	FUC	J1	63/151	63	30
		J2	61/291	72	12
		S0	50/42	30	17
4	SAA	J1	89/140	42	26
		J2	58/293	63	24
		S0	51/58	50	42
5	SAA	j1	82/352	28	38
		j2	63/210	48	32
		S0	35/070	43	52
6	SAA	j1	59/58	25	20
		j2	86/161	50	22
		S0	39/225	48	12

7	SAA	j1	69/213	37	32
		j2	79/285	51	41
		S0	22/318	35	34
8	SAA	j1	69/213	49	25
		j2	79/285	54	20
		S0	22/318	39	30
9	SAA	j1	87/236	47	37
		j2	75/163	40	32
		S0	14/334	51	25
10	SAA	j1	80/241	52	20
		j2	75/186	48	17
		S0	10/027	30	35
11	SBI	j1	73/140	39	30
		j2	81/041	42	28
		S0	16/324	50	17
12	SAA	j1	89/347	51	30
		j2	81/098	39	28
		S0	10/034	47	29

Table 3 Summary of RQD, Jv and P21 calculation for the geological Fms. analysed

ID	Geol. Fm.	RQD [%]	Jv [m/m^3]	P21 [m/m^2]
1	COI	81	6.7	9
2	CDU	80	10.6	9.1
3	FUC	68	11.5	13.8
4	SAA	61	12.5	12.7
5	SAA	45	21	18
6	SAA	45	21	18.6
7	SAA	31	26	19
8	SAA	53	18	13
9	SAA	39	23	16
10	SAA	34	25	14
11	SBI	55	18	19
12	SAA	72	13	14

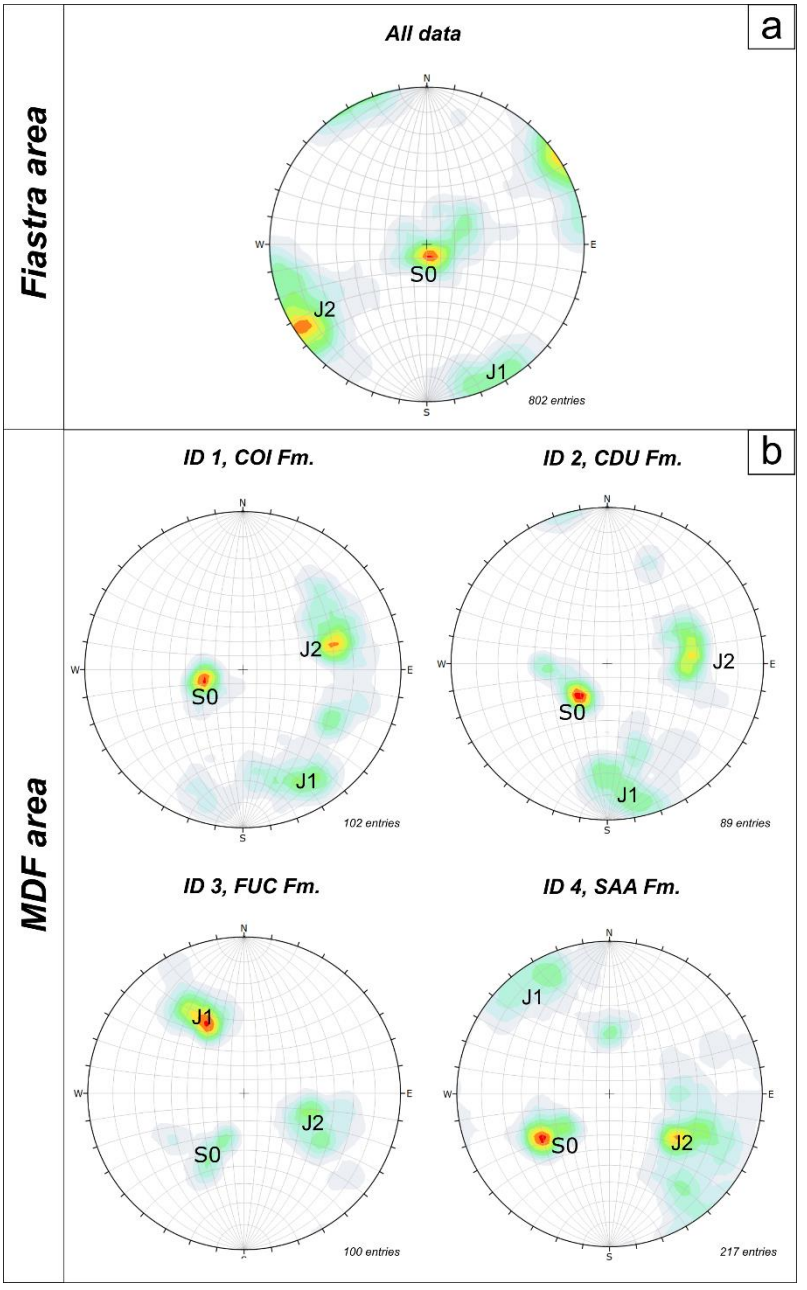

Fig. 4 Contour plot (equiareal stereographic projections, lower hemisphere) of the tectonic discontinuities belonging to the Fiastra area **(a)** and MDF area **(b)**

4.2. EQ results

During the field survey, more than 9,000 EQ rebound measurements were collected in the area. The results of data collection with the EQ are summarised in Table 4, including descriptive statistics (mean ± standard deviation, max, min) useful to verify the consistency of data obtained for each outcrop and assess hardness variability among and within rock masses. Additionally, an assessment of the percentage of the lithologies involved in the analysis is reported, as well the geological formation examined. A moderate hardness variability can be observed among the outcrops (Table 4), both in Fiastra and MDF areas. In particular, the highest average EQ values (Lavg= 700 L) and low standard deviation (dev.st = 60) can be observed for the CDU Fm., mainly composed by chert limestones. The low standard deviation highlights homogeneity of the hardness values within the outcrop and the high Lavg values recorded at this site is related to the good geotechnical properties of the chert limestones. The lowest mean hardness values (Table 4) can be observed in the marly layers of the SBI Fm. (ID 11, Lavg = 368 L), while the highest is observed in the calcarenites of CDU Fm. (ID 2, Lavg = 700 L). Focusing on the SAA formation, which is also the most investigated (8 out of 12 geomechanical measurement sites), we can see a discrete hardness variability (82 L < dev.st. < 178 L and 520 L < Lavg < 623 L).

Table 4 Summary of EQ data acquired in Marche and Abruzzo Regions, accompained with a descriptive statistics. Geological formation and lithology are reported

Id	Geol.Fm	Lithology	% of lithology	Lavg	Lmin	Lmax	Ldev.st	No. of EQ impacts
1	COI	Limestones	100	685	238	651	81	800
2	CDU	Calcarenites	100	700	374	813	60	800
3	FUC	Calcareous marls	80	620	338	664	110	640
3	FUC	Marls	20	340	167	580	190	160
4	SAA	Calcareous marls	100	602	304	660	90	800
5	SAA	Calcareous marls	100	540	487	734	92	800
6	SBI	Marls	20	368	175	560	182	160
6	SBI	Calcareous marls	80	593	232	803	111	640
7	SAA	Calcareous marls	100	520	385	696	133	800
8	SAA	Calcareous marls	100	623	478	720	140	800
9	SAA	Calcareous marls	100	580	390	690	82	800
10	SAA	Calcareous marls	100	550	347	586	167	800

11	SAA	Calcareous marls	100	559	392	703	110	800
12	SAA	Calcareous marls	100	600	428	701	178	800

4.3. Mechanical layering, degree of fracturing and the EQ rebound

This section focuses on the relationship between rock mass hardness and geomechanical indices such as P21, Jv and RQD. Single-variable linear regression models are employed to explore the individual influence of each parameter on Lavg. Furthermnore, to better capture the combined effects of these variables, multivariable regression models are introduced. These models provide deeper insights into the interdependencies between fracture intensity, joint distribution, and rock quality.

4.3.1. Single-Variable Linear Regression

The influence of the degree of rock mass fracturing on EQ rebound was tested by performing single variable linear regression models between the average value of EQ for each outcrop and the geomechanical parameters P21, Jv, and RQD (Fig. 5 and Table 5). For completeness, both Pearson's correlation coefficient (r) and coefficient of determination (R^2) are reported, together with Root Mean Squared Error (RMSE) and Mean Absolute Percentage Error (MAPE). All the regression models evidence a statistically significant (p-value ≤ 0.05) strong relationship between all the variables examined ($R^2 > 0.75$, $|r| > 0.87$). In Fig. 5 a positive association is observed for Lavg *vs.* RQD, while a negative association is evidenced for Lavg *vs.* P21 and Jv. The strongest correlation is observed for Lavg *vs.* P21 ($R^2 = 0.80$, $|r| = 0.89$).

4.3.2. Multivariable Linear Regression

To further strengthen the analysis and account for the combined influence of multiple geomechanical indices, multivariable regression models were developed. These models used Lavg, RQD, Jv, and P21 as independent variables to predict each dependent variable (e.g., P21, Jv, and RQD). As reported in Table 5, the multivariable regression models produced stronger predictive relationships compared to single-variable linear regression. For example, when

predicting Lavg based on RQD, Jv, and P21, the R-squared value increased to 0.87, indicating a significant improvement over the single-variable models. Specifically, the single-variable predictions yielded R-squared values of 0.76 for RQD, 0.75 for Jv, and 0.80 for P21. Additionally, the root mean squared error (RMSE) and mean absolute percentage error (MAPE) were reduced across the models. For instance, the RMSE for the model predicting Lavg based on RQD, Jv and P21 was 19.13, with a MAPE of 2.69%, indicating a better fit and accuracy compared to the simpler single-variable models. These improvements in R-squared values, coupled with reduced RMSE and MAPE, demonstrate that including multiple variables in the regression analysis provides a more comprehensive understanding of the factors influencing rock mass hardness and fracture density, suggesting that the multivariable models are superior at capturing the complexity of the relationships between geomechanical parameters and Lavg.

Table 5 Synthesis of regression parameters (R^2 and r) of variables Lavg, Jv, P21, RQD. p-value, RMSE and MAPE are reported.

Regression method	Variables (dependent vs. independent)	r	R^2	p-values	RMSE	MAPE (%)	Regression equation
Single-Variable Linear Regression	Lavg *vs.* RQD (Deere 1963)	0.87	0.76	0.0002	9.68	15.68	Lavg = 0.2489 RQD - 92.629
	Lavg *vs.* Jv	-0.87	0.75	0.0003	3.75	22.33	Lavg = - 0.0893 Jv + 70.289
	Lavg *vs.* P21	-0.89	0.80	0.00001	1.48	7.71	Lavg = - 0.0503 P21 + 44.478
Multivariable Linear Regression	Lavg vs. RQD and Jv	0.82	0.66	0.0021, 0.0009	31.42	4.67	Lavg = 332.5848 * RQD + 3.7078 * Jv
	Lavg vs. RQD and P21	0.92	0.85	0.0000, 0.0001, 0.0000	20.83	2.92	Lavg = 688.8132 * RQD + 1.0191 * P21 - 10.6211
	Lavg vs. Jv and P21	0.91	0.83	0.0000, 0.0021, 0.0000	22.25	3.05	Lavg = 794.8640 * Jv - 2.0471 * P21 - 11.6064
	Lavg vs. RQD, Jv and P21	0.93	0.87	0.0000, 0.0001, 0.0008, 0.0000	19.13	2.69	Lavg = 457.8320 * RQD + 3.2894 * Jv + 6.7152 * P21 - 11.3081

In addition to these results, it is important to emphasize the role of combining multiple factors to capture the intricate interdependencies within the rock mass properties. This can be seen at the scale of the outcrop in Fig. 6 (outcrop ID 11, Fig. 1. Table 1), where the distribution of EQ values for 3 different sampling windows is plotted together with the

P21 parameter and the spatial distribution of the multi-layered geological formation composed by marly limestones (in the amount of 80% of the total) and marls (about the 20% of the total). The spatial interpolation of the EQ values was performed via the Inverse Distance Weighting (IDW) approach on the two lithologies. The marly layers exhibit relatively low hardness, with an Lavg ranging from 200 L to 550 L, whereas marly limestones have EQ values ranging from 300 L to 800 L. This highlights how the degree of fracturing within the same rock mass influences the EQ weighted average values. In fact, the P21 computed in three separate sampling windows (1, 2 and 3 in Fig. 6), is inversely related to the EQ average value calculated in the same sampling windows. In details, sampling window 1 (1 in Fig. 6) exhibits lower fracturing (P21 = 12 m/m^2) and higher rebound (Lavg = 614), whereas in window 2, fracturing increases significantly (P21 = 21 m/m^2), and the average EQ value declines (Lavg = 581), eventually leading to the most fractured zone of windows 3 (P21 = 23 m/m^2) with an Lavg = 466.

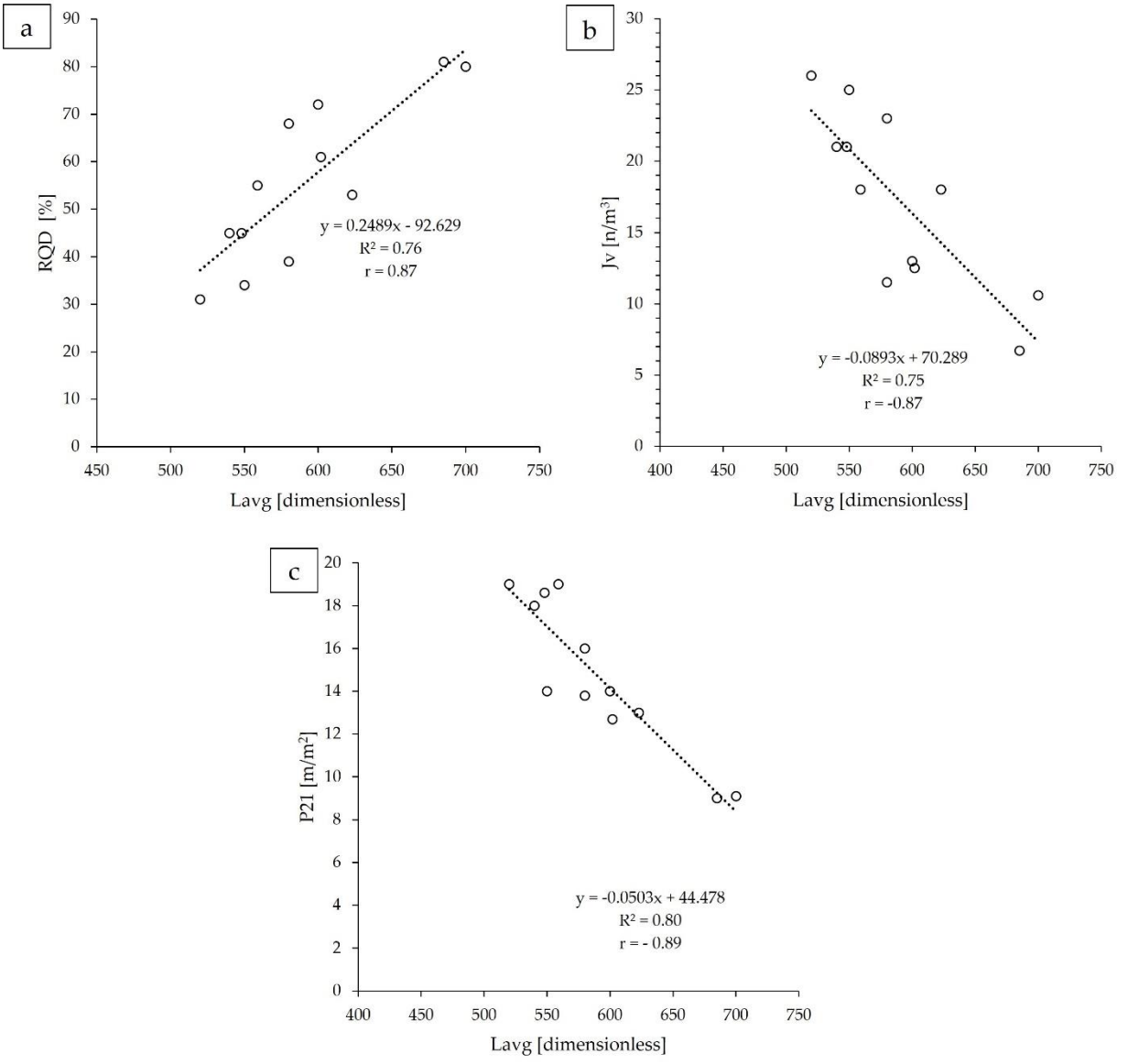

Fig. 5 Correlation between average rebound values of the EQ (Lavg) with the parameters examined. **a** Lavg vs. RQD; **b** Lavg vs. Jv; **c** Lavg vs. P21. The regression law, the Pearson's correlation coefficient (r) and Pearsons' coefficient of determination (R^2) are reported

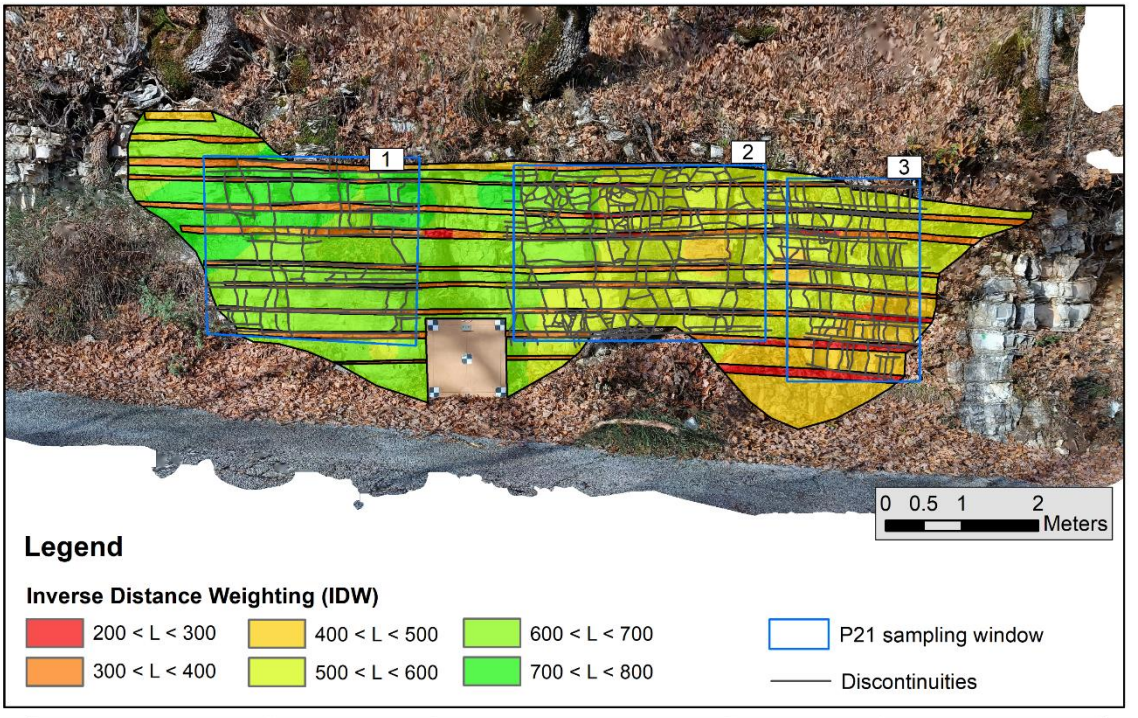

Sampling window	P21 [m/m^2]	Lavg marly limestones	Lavg marls	L avg
1	12	672	381	614
2	21	640	344	581
3	23	500	331	466

Fig. 6 Spatialization of EQ rebound values for marly and marly limestones (ID 11) layers with the IDW method. P21 sampling windows are indicated with numbers, together with discontinuities derived from the NetworkGT tool of ArcGIS

Moreover, to assess variability of EQ data within the rock masses analysed a distribution analysis has been made (Fig. 7). The approach for distribution analysis is aimed at the definition of uni- *vs*. bi-modality and can be assessed through a variety of indexes, such as the bimodality coefficient (BC in Fig. 7) (SAS 2012) Hartigan's dip statistic (HDS) (Hartigan, 1985), and Akaike's information criterion (AIC) (Akaike 1974). Using the MATLAB® function developed by Hristo Zhivomirov (2022), the BC value has been calculated for the EQ distributions. Based on the theory described in Pfister et al. (2013), the BC value of a given empirical distribution is compared to a benchmark value of BCcrit = 5/9 ≈ 0.555, that would be expected for a uniform distribution. It can be seen that bimodal distributions (with BC > 0.55) have been gathered for those geological formations characterized by mechanical layered rock masses, i.e. SBI

and FUC (Fig. 7c, 7e). Figure 7 illustrates the bimodal distribution of EQ values across different formations, revealing critical insights into rock mass behavior. The observed bimodal patterns suggest a clear relationship between lithological characteristics and the degree of fracturing, providing evidence that certain formations are more susceptible to variations in hardness. Such distributions reinforce the notion that understanding the interplay among rock structure, weathering, and mechanical properties is essential for accurate assessments of rock mass quality.

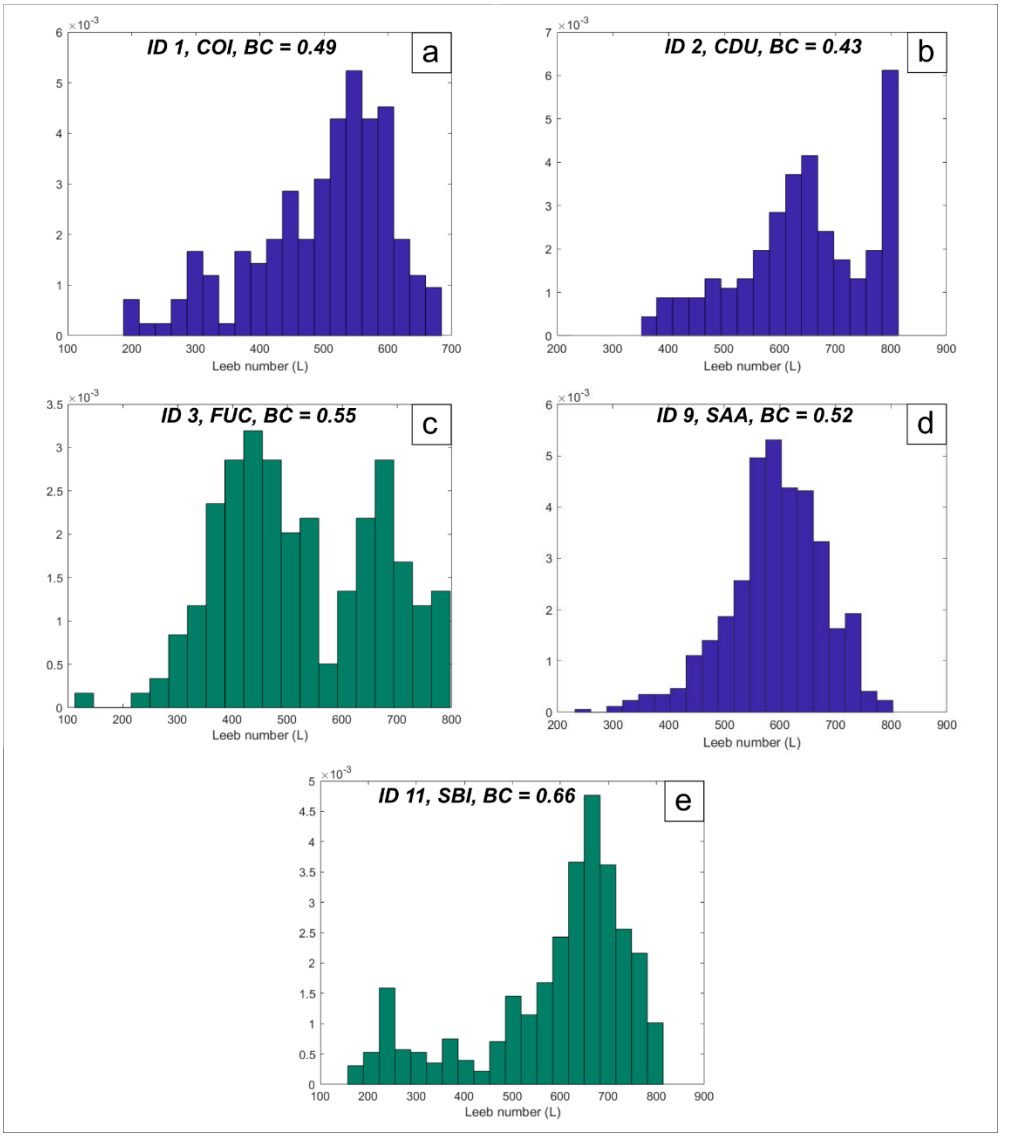

Fig. 7 Analysis of bimodal distributions for EQ data, integrating information of discontinuity density. The slope values of the interpolation lines give an indication of the discontinuity density (DD) homogeneity; **a** ID 1, COI Fm.; **b** ID 2, CDU Fm.; **c** ID 3, FUC Fm.; **d** ID 9, SAA Fm.; **e** ID 11, SBI Fm. In green the two geological Fms. with BC values above 0.55

5. Discussion

The approach proposed in this study, which is based on the application of the EQ on a regular measurement grid on the outcrop, was useful in assessing changes in rock mass hardness within and among different outcrops. To the best of our knowledge, EQ is commonly used on rock samples to determine the UCS of intact rock (Aoki and Matsukura 2008; Daniels et al. 2012; Gilbert et al. 2019; Lee 2015; Verwaal and Mulder 1993), or it is used for studies of rock surface weathering (Aoki and Matsukura 2007b; Coombes et al. 2013; Pappalardo et al. 2018; Viles et al. 2011; Wilhelm et al. 2016). Notable applications of EQ include the assessment of rock strength variation on tunnel excavation faces (Tsusaka and Tokiwa 2013), and the evaluation of rock core strength variation due to weathering, fracturing and unit weight in fracture zone landslides (Furuya 2015). However, EQ has never been used to investigate the heterogeneity of rock masses due to lithological variation and fracturing degree, in contrast to the Schmidt hammer for which few studies are available (Greco and Sorriso-Valvo 2005; Poblet et al. 2022). Rock strength variation through the Schmidt hammer at the outcrop scale have been observed by Greco and Sorriso-Valvo (2005), which observed a correlation between apparent joint spacing and Schmidt hammer rebound. Similar findings have been found by Poblet et al. (2022), who observed a negative association among the Schmidt hammer rebound and the stress endured by the rock. In this study, rock mass zoning has been evaluated applying the EQ data collection strategy based on a regular measurement grid on the outcrop, composed by 20 equally spaced measurement nodes (Disperati et al. 2012), distributed in proportion to the occurrence of different lithologies in the same outcrop. This approach focuses on the macroscopic heterogeneity driven by fractures, discontinuities, and lithological variations, which directly affect the mechanical properties of rock masses, allowing important considerations regarding the variability of rock mass hardness at outcrop scale and between different rock masses in an area. In fact, the analysis of EQ data for each outcrop revealed a high variability of rebound data, even for each specific site (Table 6), driven by lithological alternances (mechanical layering) and changes in fracturing degree. The results showed that the strongest geological formations (such as COI and CDU with Lavg ≈ 700 L) display the lowest degree of fracturing (P21 ≈ 9 m/m^2, 6.7 < Jv < 10.6

m/m^3 and RQD ≈ 80 %), coupled with the lowest standard deviation of EQ values (Ldev.st in Table 6), indicating homogeneity of EQ values within the outcrop. On the other hand, a decrease in Lavg, coupled with an increase in Ldev.st is observed on highly jointed formations (SBI and SAA Fms.), which are therefore characterised by an increase in P21, Jv and a decrease in RQD. In simple words, the higher the degree of fracturing, the greater the variability of EQ data within the same site. Focusing on the structural features, joints and dissolution cleavage surfaces represent the primary discontinuities in the formations of the study area. Spaced, disjunctive pressure-solution solution cleavage and tectonic stylolites are well developed in the more competent calcareous lithologies. On the other hand, the tectonic foliation (locally of slaty cleavage type) is more pervasive in the marly-clayey less competent strata included within calcareous-marly-clayey formations. However, in most of the analysed outcrops, the dissolution cleavage appears dilated, forming a set of planar structures with variable openings well-developed. The early development of both sets of structural discontinuities occurred during the Layer-Parallel Shortening phases (Tavani et al., 2015). This process affected crustal sectors that form Upper Messinian to Lower Pliocene, (Mazzoli et al., 2005), were located at the front of the forming chain but not yet within it. The formation of dissolution cleavage continued during the initial stages of regional fold amplification, while joints predominantly formed during the later stages of folding (Tavani et al., 2012). Moreover, the development of dissolution cleavage was more intense on the limbs of regional folds, whereas joints formed preferentially in the crestal areas (Tavani et al., 2012). As a result, the folding deformation processes intensified the structural discontinuities. According to Sari (2019) and Goudie (2016), this study confirmed that fracture intensity plays an important role in rock mass behaviour, as the higher the fracturing degree, the more fractured surfaces increase, leading to rock surface degradation and reducing intact rock uniaxial strength.

Table 6 Overview of EQ values (average and standard deviation) and degree of fracturing parameters (Jv, P21, RQD) for the geomechanical measurement sites analysed

Id	Geol.Fm	Lithology alternances	Lavg	Ldev.st	RQD %	Jv [m/m^3]	P21 [m/m^2]
1	COI	no	685	81	81	6.7	9
2	CDU	no	700	60	80	10.6	9.1
3	FUC	yes	564	150	68	11.5	13.8
4	SAA	no	602	90	61	12.5	12.7
5	SAA	no	540	92	45	21	18

6	SBI	yes	548	147	45	21	18.6
7	SAA	no	520	133	31	26	19
8	SAA	no	623	140	53	18	13
9	SAA	no	580	82	39	23	16
10	SAA	no	550	167	34	25	14
11	SAA	no	559	110	55	18	19
12	SAA	no	600	178	72	13	14

Another important aspect highlighted in this study regard the mechanical layering at outcrop scale, investigated through the bimodal distribution analysis (BC > 0.55). The analysis highlighted as in the outcrops 3 and 11 (FUC and SBI Fms, respectively) the marly layers are characterised by lower EQ values with respect to the marly limestones. This aspect is confirmed in Fig. 6, in which the spatialisation of the EQ data using the IDW method point outs the variation of EQ values by both lithology and degree of fracturing (P21).

The correlation between Lavg and the geomechanical indexes such as RQD, Jv and P21 can be observed both a local (outcrop) and regional scale. In the single-variable regression models, a high correlation is depicted, with $R^2 > 0.75$ and $|r| > 0.87$. The regression models are linear, and the p-value indicates high significance of all the relations. The strongest correlation has been found for Lavg *vs.* P21, with r = - 0.89 and $R^2 = 0.80$. This may be due to the fact that the P21 is acquired within a rectangular sampling window (2D surface) through the photogrammetric technique, whereas Jv and RQD are calculated from 1D scan lines. However, in the multivariable regression model that incorporated all three geomechanical indices (P21, Jv, and RQD), the explanatory power improved significantly, with R^2 increasing to 0.87. This demonstrates that the multivariable model better captures the combined influence of fracture intensity and rock quality, as shown by a reduction in RMSE and MAPE, further improving prediction accuracy. The multivariable model's R-squard of 0.87 compared to 0.80 for the single-variable analysis of P21 highlights the added value of considering multiple factors together.

While this study focused on sedimentary formations in the Umbria-Marche region, the principles and methodologies applied, including the use of EQ rebound data in conjunction with geomechanical indices such as RQD, Jv, and P21, are broadly applicable. However, it is important to acknowledge that certain lithological and structural characteristics

specific to other geological formations may influence the specific correlations observed in this study. For example, variations in mineralogy, fracture network geometry, and surface weathering could result in different rebound behaviors. Therefore, future applications should consider these factors when applying this methodology to new geological settings. Further studies could expand the dataset by applying the method to a broader range of formations to confirm the consistency of these findings.

6. Conclusions

This study has demonstrated the effectiveness of using the EQ hardness tester for *in-situ* hardness characterization of rock masses across a few calcareous geological formations in Central Italy. By systematically collecting more than 9,000 EQ rebound measurements and correlating them with geomechanical indices such as RQD, Jv, and P21, the research provided valuable insights into how lithological variations and the degree of fracturing influence rock mass hardness. The results quantitatively highlight the influence of fracture density on rock hardness, with the highest EQ values observed in formations with lower degrees of fracturing (e.g., CDU formation with Lavg = 700 L, RQD = 80%, and Jv = 10.6), and the lowest values in highly fractured formations (e.g., SBI formation with Lavg = 368 L, RQD = 45%, and Jv = 21). The multivariable regression models produced stronger predictive relationships, with R^2 values up to 0.87, compared to the single-variable models. This indicates that combining multiple geomechanical indices (P21, Jv, and RQD) provides a more comprehensive and accurate understanding of the factors influencing rock mass hardness. The multivariable regression results, with higher R^2 and reduced RMSE and MAPE, further emphasize the importance of using combined approaches to improve the reliability and precision of predictions regarding rock mass behavior.

Furthermore, this research emphasizes the importance of using spatially distributed grids to collect EQ data, allowing for a more comprehensive assessment of rock mass hardness and its variability at both the outcrop and regional scales. This approach significantly reduces data collection subjectivity and provides a robust statistical basis for evaluating rock mass quality. Additionally, our results underscore the need to account for mechanical layering and fracturing when using EQ measurements to estimate rock mass strength, as these factors directly affect hardness and,

consequently, the uniaxial compressive strength of rock masses. Future researches should focus on applying this approach to a broader range of geological formations and environments to validate its versatility and robustness. By expanding the dataset and testing in varied lithological and structural conditions, the methodology could offer deeper insights into rock mass behaviour. Additionally, integrating this technique with other non-destructive testing methods or advanced modelling could further refine its accuracy. Such advancements would not only enhance its applicability but also contribute more significantly to hazard management and engineering design across several geomechanical scenarios.

Acknowledgements

The authors acknowledge CIIP Spa for supporting this research.

Declarations

Competing interests The authors declare no competing interests.

References

Alberti AP, Gomes A, Trenhaile A, Oliveira M, Horacio J (2013) Correlating River terrace remnants using an Equotip hardness tester: An example from the Miño River, northwestern Iberian Peninsula. Geomorphology 192, 59–70. https://doi.org/10.1016/j.geomorph.2013.03.017

Aldeeky, H., Al Hattamleh, O., & Rababah, S. (2020). Assessing the uniaxial compressive strength and tangent Young's modulus of basalt rock using the Leeb rebound hardness test. Materiales de Construcción, 70(340), e230-e230.

Akaike H (1974) A new look at the statistical model identification. IEEE transactions on automatic control, 19(6), 716-723.

Aoki H, Matsukura Y (2008) Estimating the unconfined compressive strength of intact rocks from Equotip hardness. Bull. Eng. Geol. Environ. 67, 23–29. https://doi.org/10.1007/s10064-007-0116-z

Aoki H, Matsukura Y (2007a) A new technique for non-destructive field measurement of rock-surface strength: an application of the Equotip hardness tester to weathering studies. Earth Surf. Process. Landf. 32, 1759–1769.

https://doi.org/10.1002/esp.1492

Aoki H, Matsukura Y (2007b) A new technique for non-destructive field measurement of rock-surface strength: an application of the Equotip hardness tester to weathering studies. Earth Surf. Process. Landf. J. Br. Geomorphol. Res. Group 32, 1759–1769

Arman H, Hashem W, Abdelghany O, Aldahan A (2013) On the accuracy of the in-situ Schmidt hammer test on carbonate rocks, in: ISRM EUROCK. ISRM, p. ISRM-EUROCK-2013-025.

Barton N (1973) Review of a new shear-strength criterion for rock joints. Eng. Geol. 7, 287–332.

Barton N, Choubey V (1977) The shear strength of rock joints in theory and practice. Rock Mech. 10, 1–54.

Birch JS (2006) Using 3DM Analyst mine mapping suite for rock face characterization. Laser Photogramm. Methods Rock Face Charact. 15.

Calamita F, Deiana G (1986) Evoluzione strutturale neogenico-quaternaria dell'Appennino Umbro-Marchigiano.

Calamita F, Pace P, Scisciani V, Properzi F, Francioni M (2021) Dinaric up-thrusts in the Pliocene evolution of the Central Apennines thrust belt of Italy: the Montagna dei Fiori structure. Geol. Mag. 158, 2063–2078. https://doi.org/10.1017/S0016756821000613

Calamita F, Pizzi A, Ridolfi M, Rusciadelli G, Scisciani V (1998) Il buttressing delle faglie sinsedimentarie pre-thrusting sulla strutturazione neogenica della catena appenninica; l'esempio della M. gna dei Fiori (Appennino centrale esterno). Boll. Della Soc. Geol. Ital. 117, 725–745.

Coombes MA, Feal-Pérez A, Naylor LA, Wilhelm K (2013) A non-destructive tool for detecting changes in the hardness of engineering materials: Application of the Equotip durometer in the coastal zone. Eng. Geol. 167, 14–19. https://doi.org/10.1016/j.enggeo.2013.10.003

Daniels G, McPhee C, McCurdy P, Sorrentino Y (2012) Non-Destructive Strength Index Testing Applications for Sand Failure Evaluation, in: All Days. Presented at the SPE Asia Pacific Oil and Gas Conference and Exhibition, SPE, Perth, Australia, p. SPE-158326-MS. https://doi.org/10.2118/158326-MS

Deere D (1963) Technical description of rock cores. Geol. u. Bauw J 28.

Dershowitz WS, Herda HH (1992) Interpretation of fracture spacing and intensity, in: The 33rd US Symposium on

Rock Mechanics (USRMS). OnePetro.

Desarnaud, J., Kiriyama, K., Simsir, B., Wilhelm, K., & Viles, H. (2019). A laboratory study of Equotip surface hardness measurements on a range of sandstones: What influences the values and what do they mean?. Earth Surface Processes and Landforms, 44, 1419 - 1429. https://doi.org/10.1002/esp.4584.

Di Francesco L, Fabbi S, Santantonio M, Bigi S, Poblet J (2010) Contribution of different kinematic models and a complex Jurassic stratigraphy in the construction of a forward model for the Montagna dei Fiori fault-related fold (Central Apennines, Italy). Geol. J. 45, 489–505.

Disperati L, Trefolini E, Massa G, Manzo C, Palamara S (2012) Engineering geological mapping in Tuscany (Italy), in: 34th International Geological Congress.

Francioni M, Simone M, Stead D, Sciarra N, Mataloni G, Calamita F (2019) A new fast and low-cost photogrammetry method for the engineering characterization of rock slopes. Remote Sensing, 11(11), 1267.

Furuya, T., & Jiang, J. C. (2015). Determination Of Slip Surfaces In Fracture Zone Landslides Using Oriented Borehole Core Samples. *GEOMATE Journal*, *8*(15), 1151-1158.

Gilbert O, Mol L, Campbell O, Blenkinsop T (2019) Permeability and Surface Hardness Surveying of Stone Damaged by Ballistic Impact. Heritage 2, 1369–1389. https://doi.org/10.3390/heritage2020087

Goudie AS (2016) Quantification of rock control in geomorphology. Earth-Sci. Rev. 159, 374–387.

Guan, S., Cao, R., Zhong, Y., Nan, H., & Wu, F. (2024). Comparison and combination of Leeb hardness and point load strength for indirect measuring tensile and compressive strength of rocks. Bulletin of Engineering Geology and the Environment, 83(4), 109.

Greco R, Sorriso-Valvo M (2005) Relationships between joint apparent separation, Schmidt hammer rebound value, and distance to faults, in rocky outcrops, Calabria, Southern Italy. Eng. Geol. 78, 309–320. https://doi.org/10.1016/j.enggeo.2005.01.003

Guerriero V, Dati F, Giorgioni M, Iannace A, Mazzoli S, Vitale S (2015) The role of stratabound fractures for fluid migration pathways and storage in well-bedded carbonates. Ital. J. Geosci. 134, 383–395.

Einstein HH, Veneziano D, Baecher GB, O'reilly KJ (1983) The effect of discontinuity persistence on rock slope stability. In International journal of rock mechanics and mining sciences & geomechanics abstracts (Vol. 20, No. 5, pp. 227-236). Pergamon.

Hartigan JA, Hartigan PM (1985) The dip test of unimodality. The annals of Statistics, 70-84.

Hristo Zhivomirov (2022) Bimodality Coefficient Calculation with Matlab https://www.mathworks.com/matlabcentral/fileexchange/84933-bimodality-coefficient-calculation-with-matlab), MATLAB Central File Exchange. Retrieved February 11, 2022.

Hujer WH, Finkbeiner T, Persaud M (2014) Estimating Rock Strength From Non-Destructive Strength Testing (EQUOTIP) and Related Benefits, in: EAGE Workshop on Geomechanics in the Oil and Gas Industry. Presented at the EAGE Workshop on Geomechanics in the Oil and Gas Industry, European Association of Geoscientists & Engineers, Dubai, United Arab Emirates,. https://doi.org/10.3997/2214-4609.20140444

Katz O, Reches Z, Roegiers JC (2000) Evaluation of mechanical rock properties using a Schmidt Hammer. Int. J. Rock Mech. Min. Sci. 37, 723–728. https://doi.org/10.1016/S1365-1609(00)00004-6

Kim T, Jeon S. (2019) Experimental study on shear behavior of a rock discontinuity under various thermal, hydraulic and mechanical conditions. Rock Mechanics and Rock Engineering, 52(7), 2207-2226.

Lee JS (2015) Calibration of Rebound Hardness Numbers to Unconfined Compressive Strength in Shale Formations. J. Pet. Technol. 67, 41–45. https://doi.org/10.2118/0115-0041-JPT

Liu, B., Schieber, J., Mastalerz, M., & Teng, J. (2020). Variability of rock mechanical properties in the sequence stratigraphic context of the Upper Devonian New Albany Shale, Illinois Basin. *Marine and Petroleum Geology*, *112*, 104068.

Mammoliti E, Di Stefano F, Fronzi D, Mancini A, Malinverni ES, Tazioli A (2022) A machine learning approach to extract rock mass discontinuity orientation and spacing, from laser scanner point clouds. Remote Sensing, 14(10), 2365.

Mammoliti E, Ferretti A, Malavolta M, Teloni R, Ruggeri P, Roselli G (2021) Defining a Non-Destructive In Situ Approach for the Determination of Historical Mortar Strength Using the Equotip Hardness Tester. Appl.

Sci. 11, 4788. https://doi.org/10.3390/app11114788

Mammoliti E, Pepi A, Fronzi D, Morelli S, Volatili T, Tazioli A, Francioni M (2023) 3D Discrete Fracture Network Modelling from UAV Imagery Coupled with Tracer Tests to Assess Fracture Conductivity in an Unstable Rock Slope: Implications for Rockfall Phenomena. Remote Sensing, 15(5), 1222.

Mattei M (1987) Analisi geologico-strutturale della montagna dei fiori (Ascoli Piceno, Italia centrale). Geol. Romana 26, 327–347.

Mazzoli S, Deiana G, Galdenzi S, Cello G (2002) Miocene fault-controlled sedimentation and thrust propagation in the previously faulted external zones of the Umbria-Marche Apennines, Italy. EGU Stephan Mueller Special Publication Series, 1, 195-209. https://doi.org/10.5194/smsps-1-195-2002

Mazzoli, S., Pierantoni, P. P., Borraccini, F., Paltrinieri, W., & Deiana, G. (2005). Geometry, segmentation pattern and displacement variations along a major Apennine thrust zone, central Italy. *Journal of Structural Geology*, *27*(11), 1940-1953.

McGinnis RN, Ferrill DA, Morris AP, Smart KJ, Lehrmann D (2017) Mechanical stratigraphic controls on natural fracture spacing and penetration. J. Struct. Geol. 95, 160–170.

Morris AP, Ferrill DA, McGinnis RN (2009) Mechanical stratigraphy and faulting in Cretaceous carbonates. AAPG Bull. 93, 1459–1470.

Nyberg B, Nixon CW, Sanderson DJ (2018) NetworkGT: A GIS tool for geometric and topological analysis of two-dimensional fracture networks. Geosphere 14, 1618–1634.

Palmstrom A (2005) Measurements of and correlations between block size and rock quality designation (RQD). Tunn. Undergr. Space Technol. 20, 362–377. https://doi.org/10.1016/j.tust.2005.01.005

Pappalardo M, Maggi E, Geppini C, Pannacciulli F (2018) Bioerosive and bioprotective role of barnacles on rocky shores. Sci. Total Environ. 619, 83–92.

Pierantoni P, Deiana G, Galdenzi S (2013) Stratigraphic and structural features of the Sibillini mountains (Umbria-Marche Apennines, Italy). Ital. J. Geosci. 132, 497–520.

Poblet J, Bulnes M, Uzkeda H, Magán M (2022) Using the Schmidt hammer on folds: An example from the

Cantabrian Zone (NW Iberian Peninsula). J. Struct. Geol. 155, 104512. https://doi.org/10.1016/j.jsg.2022.104512

Proceq SA (1977) Equotip operations instructions. Zurich PROCEQ SA.

Ritz, E., Honarpour, M. M., Dvorkin, J., & Dula, W. F. (2014, August). Core hardness testing and data integration for unconventionals. In SPE/AAPG/SEG Unconventional Resources Technology Conference (pp. URTEC-1916004). URTEC.

Sakız, U. (2024). Predicting the brittleness of sandstones from the Leeb hardness test. Petroleum Science and Technology, 42(11), 1360-1384.

Sari M (2019) Incorporation of uncertainty in estimating the rock mass uniaxial strength using a fuzzy inference system. Arab. J. Geosci. 12, 18. https://doi.org/10.1007/s12517-018-4169-z

Scisciani V, Tavarnelli E, Calamita F (2002) The interaction of extensional and contractional deformations in the outer zones of the Central Apennines, Italy. J. Struct. Geol. 24, 1647–1658.

Shackleton JR, Cooke ML, Sussman AJ (2005) Evidence for temporally changing mechanical stratigraphy and effects on joint-network architecture. Geology 33, 101–104.

Shang J, West LJ, Hencher SR, Zhao Z (2018) Geological discontinuity persistence: Implications and quantification. Engineering Geology, 241, 41-54.

Storti F, Balsamo F, Koopman A (2017) Geological map of the partially dolomitized Jurassic succession exposed in the core of the Montagna dei Fiori Anticline, Central Apennines, Italy. Ital. J. Geosci. 136, 125–135.

Sumner P, Nel W (2002) The effect of rock moisture on Schmidt hammer rebound: tests on rock samples from Marion Island and South Africa. Earth Surf. Process. Landf. 27, 1137–1142. https://doi.org/10.1002/esp.402

Tasse, E., Gallant, K., Veltin, K., & Ducharme-Rivest, S. (2024, September). Utilising Equotip Leeb hardness testing for rock strength estimation and geotechnical domain definition. In Deep Mining 2024: Proceedings of the 10th International Conference on Deep and High Stress Mining (pp. 1079-1090).

Tavani, S., Storti, F., Bausa, J., & Munoz, J. A. (2012). Late thrusting extensional collapse at the mountain front of

650 the northern Apennines (Italy). *Tectonics*, *31*(4).
651 Tavani, S., Storti, F., Lacombe, O., Corradetti, A., Muñoz, J. A., & Mazzoli, S. (2015). A review of deformation
652 pattern templates in foreland basin systems and fold-and-thrust belts: Implications for the state of stress in
653 the frontal regions of thrust wedges. *Earth-Science Reviews*, *141*, 82-104.
654 Thrower, A., Barlow, J., Moore, R., & Cane, T. (2022). A pilot study investigating the rapid estimation of intact dry
655 density of chalk using low impact energy hardness measurements taken with an Equotip Leeb hardness
656 tester. Quarterly Journal of Engineering Geology and Hydrogeology, 55(2), qjegh2021-101.
657 Torabi A, Alaei B, Ellingsen TSS (2018) Faults and fractures in basement rocks, their architecture, petrophysical
658 and mechanical properties. J. Struct. Geol. 117, 256–263.
659 Tozer RSJ, Butler RWH, Chiappini M, Corrado S, Mazzoli S, Speranza F (2006) Testing thrust tectonic models at
660 mountain fronts: where has the displacement gone? Journal of the Geological Society, London, 162, 1–14.
661 https://doi.org/10.1144/0016-764904-140
662 Tsusaka K, Tokiwa T (2013) Influence of fracture orientation on excavatability of soft sedimentary rock using a
663 hydraulic impact hammer: A case study in the Horonobe Underground Research Laboratory. Tunn.
664 Undergr. Space Technol. 38, 542–549. https://doi.org/10.1016/j.tust.2013.08.007
665 Verwaal W, Mulder A (1993) Estimating rock strength with the Equotip hardness tester, in: International Journal of
666 Rock Mechanics and Mining Sciences and Geomechanics Abstracts. Elsevier Science, pp. 659–662.
667 Viles H, Goudie A, Grab S, Lalley J (2011) The use of the Schmidt Hammer and Equotip for rock hardness
668 assessment in geomorphology and heritage science: a comparative analysis. Earth Surf. Process. Landf. 36,
669 320–333. https://doi.org/10.1002/esp.2040
670 Wakasa S, Matsuzaki H, Tanaka Y, Matsukura Y (2006) Estimation of episodic exfoliation rates of rock sheets on
671 a granite dome in Korea from cosmogenic nuclide analysis. Earth Surf Proc Land 31:1246–1256
672 Watkins H, Healy D, Bond CE, Butler RW (2018) Implications of heterogeneous fracture distribution on reservoir
673 quality; an analogue from the Torridon Group sandstone, Moine Thrust Belt, NW Scotland. J. Struct. Geol.
674 108, 180–197.

Wilhelm K, Viles H, Burke Ó (2016) Low impact surface hardness testing (Equotip) on porous surfaces - advances in methodology with implications for rock weathering and stone deterioration research: Equotip Hardness Testing on Porous Rock and Stone. Earth Surf. Process. Landf. 41, 1027–1038. https://doi.org/10.1002/esp.3882

Yılmaz, N. G. (2013). The influence of testing procedures on uniaxial compressive strength prediction of carbonate rocks from Equotip hardness tester (EHT) and proposal of a new testing methodology: hybrid dynamic hardness (HDH). Rock mechanics and rock engineering, 46, 95-106.

Yilmaz, N. G., & Goktan, R. M. (2019). Comparison and combination of two NDT methods with implications for compressive strength evaluation of selected masonry and building stones. Bulletin of Engineering Geology and the Environment, 78, 4493-4503.